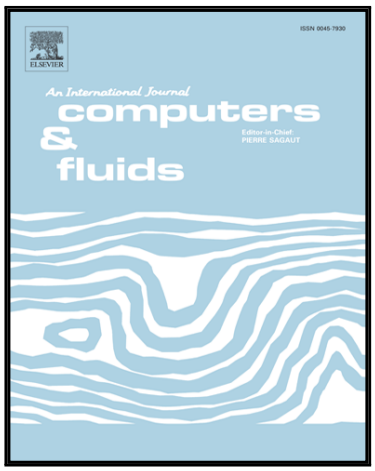


# Boundary conditions with adjustable slip length for the lattice Boltzmann simulation of liquid flow

Liuming Yang, Yang Yu, Guoxiang Hou, Kai Wang, Yeping Xiong

PII: S0045-7930(18)30437-7
DOI: https://doi.org/10.1016/j.compfluid.2018.08.002
Reference: CAF 3967

To appear in: *Computers and Fluids*

Received date: 4 June 2018
Revised date: 13 July 2018
Accepted date: 6 August 2018

Please cite this article as: Liuming Yang, Yang Yu, Guoxiang Hou, Kai Wang, Yeping Xiong, Boundary conditions with adjustable slip length for the lattice Boltzmann simulation of liquid flow, *Computers and Fluids* (2018), doi: https://doi.org/10.1016/j.compfluid.2018.08.002

**Highlights**

- Four slip boundary conditions are presented for liquid flow.
- The proposed schemes surmount the barrier of limited slip length.
- The proposed schemes are specified by the slip length.
- Two slip boundary conditions are suitable for curved walls.

# Boundary conditions with adjustable slip length for the lattice Boltzmann simulation of liquid flow

Liuming Yang[a], Yang Yu[a], Guoxiang Hou[a,*], Kai Wang[a], Yeping Xiong[b]

[a] *School of Naval Architecture and Ocean Engineering, Huazhong University of Science and Technology, Wuhan, 430074, People's Republic of China*

[b] *Faculty of Engineering and the Environment, Boldrewood Innovation Campus, University of Southampton, Southampton, SO16 7QF, UK*

**Abstract**

The phenomenon of liquid slip has been studied by many researchers using the lattice Boltzmann method. However, boundary conditions for the lattice Boltzmann simulation of liquid flow are far from perfect and how to specify the boundary conditions for liquid flow with slip accurately is still a challenge. In this work, we introduce four widely used slip boundary conditions in gaseous flow into the simulation of liquid flow, two half-way schemes and two modified schemes. Theoretical analysis shows that all half-way schemes are equivalent in principle, so are the modified schemes. According to the equivalence of these schemes, these slip boundary conditions are improved by expanding the range of the combination parameters from [0,1] to [0,2] to surmount the barrier of limited simulated slip length. And the relations between the combination parameters and the slip length are deduced strictly in theory. The specified combination parameter is decided by the given slip length and the relaxation time. The discrete effects of these slip boundary conditions are analysed. If the grid is fine enough, the discrete effects can be ignorable and the local flow at the wall can be approximated as flow with linear velocity gradient. The accuracy and reliability of our method have been verified by the simulations of the Couette flow, the Poiseuille flow and the unsteady Womersley flow. The cylindrical Couette flow is also implemented to explore the possibility of simulating liquid flows with curved boundary.

*Keywords:* liquid slip boundary conditions, Navier's slip model, slip length, lattice Boltzmann simulation

*Guoxiang Hou

*Email address:* houguoxiang@163.com (Guoxiang Hou)

## 1. Introduction

Friction reduction has always been a hot topic for naval architecture and marine engineering. With the rapid development of micro-nano-technology, liquid flow at micro-scale has attracted increasing attention [1, 2]. Smaller friction force is beneficial to micro devices. One of ways to reduce friction is to make use of superhydrophobic surfaces [3, 4, 5]. The development of the chemical science engineering makes it possible to obtain superhydrophobic surfaces with special chemical properties and microstructures [6, 7, 8, 9]. Superhydrophobic surfaces possess numerous micro-grooves, which entrap air when the surfaces are fully submerged in liquid [10, 11]. So the physical boundary of a liquid flow is composed of liquid-solid and liquid-air interfaces. Appreciable apparent liquid slip will emerge with suitable liquid-air interfaces [12, 13]. To quantify the boundary slip, Navier proposed the concept of 'slip length' [14], which is commonly accepted by researchers nowadays [15]. With the assumption of the linear slip model, slip length is defined as the ratio of the slip velocity to the absolute value of the velocity gradient in the normal direction of the wall. The non-dimensional form of the Navier's slip model is also presented in the following researches [16]. To study the phenomenon of boundary slip, many experiments were carried out with surface force apparatus, atomic force microscopy, particle image velocimetry, and Quartz crystal resonators techniques [17]. These instruments are still not accurate enough at micro-nano-scale. Numerical methods show their potential to make up for the deficiency of experiments. Karimipour et al. simulated the water-Cu nanofluid considering the influences of the nanofluid Richardson number and the nanoparticles volume fraction [18]. Besides, simulation is necessary to explore the mechanism about the slip length. By numerical simulations, Esfandiary et al. studied the Brownian motion and thermophoresis effect to explore the mechanisms of slip velocity [19]. The conclusion will inspire researchers to obtain the desired slip length and utilize the slip phenomenon.

The lattice Boltzmann method (LBM) is a promising tool to simulate micro liquid flow with boundary slip. The lattice Boltzmann equation is derived from the Boltzmann equation without the continuum assumption and needs less computing time than the molecular dynamics simulation because of its kinetic particle nature, local calculation and natural parallelism [20, 21]. In recent years, researchers have done many work in the slip boundary conditions of the LBM. Nie et al. employed the bounce-back boundary condition of LBM to simulate fluid flow in Micro-electro-mechanical systems and cap-

tured the behavior of velocity slip [1]. But later researchers found that it is because of the discrete effect of the bounce-back scheme [22]. Lim et al. used the specular reflection boundary condition to simulate microchannel flows [2]. The slip velocity they obtained differs from some analytical results. Then Succi proposed a combination of bounce-back and specular (BSR) scheme to capture velocity slip on solid walls [23]. As shown in his work, the degree of slip is highly dependent on the combination parameter $r$ ($0 \leq r \leq 1$). In order to investigate the gravity effect, Karimipour et al. included a force part into the BSR scheme to simulate the slip velocity accurately [24]. Tang et al. developed a more general diffuse boundary condition which is the combination of the discrete full diffusive and specular reflection(DSR) boundary condition [25, 26]. Researchers found that slip velocity predicted by the DSR scheme is bigger than physical results in some cases [27]. Recently, Chai et al. and Verhaeghe et al. put forward a new scheme which is the combination of the discrete full diffusive and bounce-back (DBB) boundary condition [28, 29]. What should be mentioned is, analysis indicates that the BSR scheme can simulate a wider range of slip velocity than the DSR scheme and the DBB scheme [20, 28].

Researchers have found a way to obtain the specified accurate combination parameter for microscale gas flow [20, 28, 30]. But for liquid micro-flow, the Knudesn number is so small that the strategy used in gas flow to choose the combination parameter can not work again. As a matter of fact, the boundary slip of liquid flow can be quantified by the slip length. With given slip length, it is reasonable to obtain a specified liquid micro-flow. Karimipour et al. simulated the nanofluid in a microchannel in slip flow regime [31, 32]. The combination parameter was chose from 0.005 to 0.05. Wang et al. studied the boundary slip phenomenon on the liquid-solid surface with the half-way BSR scheme and the formula of adhesion force [33]. The combination parameter was given by trial and error. Ahmmed et al. found that the slip length ($b$) can be related to the combination parameter by the power law. The prefactor and the exponent were determined by numerical fitting [34]. *Švec* et al. also obtained an approximate equation relating the combination parameter with the slip length [35]. In fact, Ahmmed et al. adopted the modified BSR scheme while *Švec* et al. used the half-way BSR scheme. They all ignored the discrete effect of the BSR scheme. An accurate relationship between the combination parameter and the slip length are essential and needs to be deduced strictly in theory. Recently, Wang et al. studied the BSR scheme for the simulation of slip in liquid flow and they

related the slip length and the relaxation factor to the combined parameter based on the Couette flow and the Navier's slip model [36]. But it is challenging to apply the BSR scheme to curved walls. So the BSR scheme is not enough for the simulation of liquid flow. The DBB scheme has more potential in the simulation of fluid flows with complex geometries for the nature of its local calculations [37, 38]. However, few simulations employed the DSR and DBB schemes for liquid flow. The main obstacle is that the DSR scheme assumes that the two extreme cases of the interaction between molecules and walls are the full diffusive and specular reflection boundary conditions and the DBB scheme assumes the two extreme cases are the full diffusive and bounce back boundary conditions [26, 28]. So the combination parameter can only vary from zero to one. As a result, both of the DSR and DBB schemes can only realize a limited range of slip length.

In order to break the limit of applying the DSR and DBB schemes into the simulation of liquid flow, we theoretically analyse these boundary conditions in the case of unidirectional liquid flow. According to the analysis, the DSR, DBB schemes are improved by expanding the range of the combination parameter from [0,1] to [0,2]. Then to specify the boundary condition, the relations between the combination parameter and slip length are deduced strictly in theory. The discrete effects of boundary conditions existing in nonlinear flow are discussed. Finally, simulations of Couette flow and Poiseuille flow are conducted to verify the accuracy and reliability of our method. We also apply the DBB schemes to the unsteady Womersley flow and the cylindrical Couette flow. Numerical results are very close to the analytical solutions.

The rest of this paper is organized as follows: in Section.2, we study the boundary conditions with adjustable slip length for LBM in theory. In Section.3, we present the numerical validation and the discussion of results. Finally, in Section.4, we get the conclusions and propose some directions for future work.

## 2. Numerical methods

The lattice Boltzmann method is a discrete approximation of the continuous Boltzmann equation. It has been recognized as an effective way for the simulation of micro-flow [39]. In this section, the lattice Boltzmann method is simply introduced and slip boundary conditions for liquid flows are proposed and analysed.

*2.1. The lattice Boltzmann method*

The evolution equation of the lattice Botlzmann method is [39]:

$$f_i(\vec{x}+\vec{e}_i\Delta t, t+\Delta t) - f_i(\vec{x},t) = -\frac{1}{\tau}[f_i(\vec{x},t) - f_i^{eq}(\vec{x},t)] + \Delta t F_i \tag{1}$$

where $f_i(\vec{x},t)$ is the particle distribution function with velocity $\vec{e}_i$ at position $\vec{x}$ and time $t$, $\Delta t$ is the time step, $\tau$ is the relaxation time, and $F_i$ is a forcing term accounting for the acceleration $\vec{a}$. $F_i$ is determined by [39]

$$F_i = \omega_i \rho (1 - \frac{1}{2\tau})[\frac{\vec{e}_i - \vec{u}}{c_s^2} + \frac{(\vec{e}_i \cdot \vec{u})\vec{e}_i}{c_s^4}]\vec{a} \tag{2}$$

Eq.(1) can also be divided into colliding step Eq.(3) and streaming step Eq.(4):

$$\bar{f}_i(\vec{x},t) = f_i(\vec{x},t) - \frac{1}{\tau}[f_i(\vec{x},t) - f_i^{eq}(\vec{x},t)] + \Delta t F_i \tag{3}$$

$$f_i(\vec{x}+\vec{e}_i\Delta t, t+\Delta t) = \bar{f}_i(\vec{x},t) \tag{4}$$

where $\bar{f}_i$ represents the post-collision distribution function.

Without losing generality, we simply choose the standard D2Q9 model for our two-dimensional simulation. The equilibrium distribution $f_i^{eq}$ of the D2Q9 is expressed as [22]

$$f_i^{eq}(\vec{x},t) = \omega_i \rho [1 + \frac{\vec{e}_i \cdot \vec{u}}{c_s^2} + \frac{(\vec{e}_i \cdot \vec{u})^2}{2c_s^4} - \frac{\vec{u}^2}{2c_s^2}] \tag{5}$$

Here $c_s$ is calculated by $c_s = \frac{c}{\sqrt{3}}$, where $c = \frac{\Delta x}{\Delta t}$ ( $\Delta x$ : lattice spacing). We set $\Delta x = \Delta t = 1$ in this paper. Besides, $\omega_i$ represents the model-dependent weight coefficients expressed as

$$\omega_i = \begin{cases} 4/9, & i = 0. \\ 1/9, & i = 1,2,3,4. \\ 1/36, & i = 5,6,7,8. \end{cases}$$

The discrete velocities of the D2Q9 model are given by

$$\vec{e}_i = \begin{cases} (0,0), & i = 0. \\ (\cos\frac{(i-1)\pi}{2}, \sin\frac{(i-1)\pi}{2})c, & i = 1,2,3,4. \\ \sqrt{2}(\cos\frac{(2i-1)\pi}{4}, \sin\frac{(2i-1)\pi}{4})c, & i = 5,6,7,8. \end{cases}$$

The macroscopic variables, density $\rho$ and velocity $\vec{u}$ in the simulation of LBM are calculated by

$$\rho = \sum_i f_i, \qquad \rho\vec{u} = \sum_i \vec{e}_i f_i + \frac{\Delta t \cdot \vec{a}}{2} \tag{6}$$

In order to simulate liquid microflows, $\tau$ is determined by liquid viscosity $\nu$ with the following relation

$$\tau = \frac{\nu}{c_s^2 \Delta t} + \frac{1}{2} \tag{7}$$

### *2.2. Slip boundary conditions for LBM in gaseous flow*

Firstly, we describe three half-way slip boundary conditions, the combination of half-way bounce back and specular reflection (HBSR) scheme, the combination of discrete full diffusive and half-way specular reflection (HDSR) scheme, and the combination of discrete full diffusive and half-way bounce back (HDBB) scheme.

As shown in Fig.1, boundaries of these half-way schemes locate at $j = 0.5$ which means the boundary are placed at the half-way of the nodes. After colliding step Eq.(3), the moving step is conducted. The particle distribution functions moving from the inner flow are obtained. But the particle distribution functions moving from the wall are unknown and they need to be processed with the boundary conditions.

To fulfill boundary conditions, we need to obtain the unknown distribution functions $f_2$, $f_5$, $f_6$.

As described below, $r$, $\bar{r}$, $s$, $\bar{s}$, $q$, $\bar{q}$ are the combination parameters and they vary from 0 to 1 in gaseous flow.

For the HBSR scheme, $f_2$, $f_5$, $f_6$ are treated as

$$\begin{cases} f_2 = \bar{f}_4 \\ f_5 = r\bar{f}_7 + (1-r)\bar{f}_8 \\ f_6 = r\bar{f}_8 + (1-r)\bar{f}_7 \end{cases} \tag{8}$$

where the particle distribution functions $\bar{f}_4$, $\bar{f}_7$, $\bar{f}_8$ are given by colliding step Eq.(3).

For the HDSR scheme, $f_2$, $f_5$, $f_6$ are expressed

$$\begin{cases} f_2 = qf_2^{eq} + (1-q)\bar{f}_4 \\ f_5 = qf_5^{eq} + (1-q)\bar{f}_8 \\ f_6 = qf_6^{eq} + (1-q)\bar{f}_7 \end{cases} \tag{9}$$

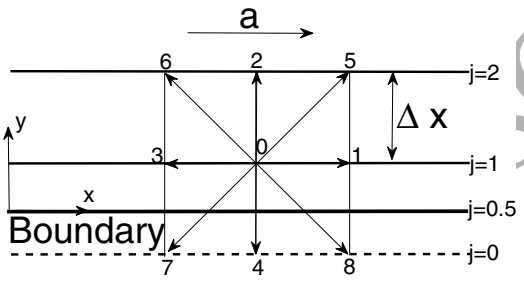


Figure 1: Lattice and boundary arrangement in the D2Q9 model for the half-way schemes

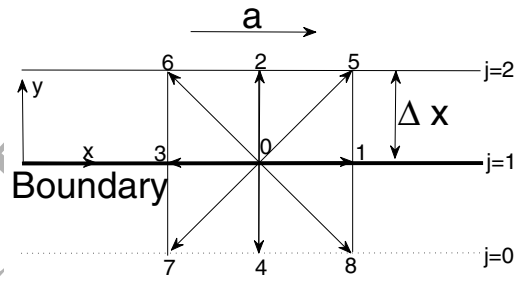


Figure 2: Lattice and boundary arrangement in the D2Q9 model for the modified schemes

For the HDBB scheme, $f_2$, $f_5$, $f_6$ are constructed as

$$\begin{cases} f_2 = sf_2^{eq} + (1-s)\bar{f}_4 \\ f_5 = sf_5^{eq} + (1-s)\bar{f}_7 \\ f_6 = sf_6^{eq} + (1-s)\bar{f}_8 \end{cases} \tag{10}$$

Then, we describe three modified slip boundary conditions, the combination of modified bounce back and specular reflection (MBSR) scheme, the combination of discrete full diffusive and modified specular refection (MDSR) scheme, and the combination of discrete full diffusive and modified bounce back (MDBB) scheme.

As shown in Fig.2, boundary nodes of the modified schemes locate at boundaries. The same as the half-way schemes, these modified schemes also need to treat the unknown distribution functions $f_2$, $f_5$, $f_6$.

For the MBSR scheme, $f_2$, $f_5$, $f_6$ are given as

$$\begin{cases} f_2 = f_4 \\ f_5 = \bar{r}f_7 + (1-\bar{r})f_8 \\ f_6 = \bar{r}f_8 + (1-\bar{r})f_7 \end{cases} \tag{11}$$

where $f_4$, $f_7$, $f_8$ are given by streaming step Eq.(4).

For the MDSR scheme, $f_2$, $f_5$, $f_6$ are treated as

$$\begin{cases} f_2 = \bar{q}f_2^{eq} + (1-\bar{q})f_4 \\ f_5 = \bar{q}f_5^{eq} + (1-\bar{q})f_8 \\ f_6 = \bar{q}f_6^{eq} + (1-\bar{q})f_7 \end{cases} \tag{12}$$

For the MDBB scheme, $f_2$, $f_5$, $f_6$ are constructed as

$$\begin{cases} f_2 = \bar{s}f_2^{eq} + (1-\bar{s})f_4 \\ f_5 = \bar{s}f_5^{eq} + (1-\bar{s})f_7 \\ f_6 = \bar{s}f_6^{eq} + (1-\bar{s})f_8 \end{cases} \tag{13}$$

With these slip boundary conditions at hand, the unknown distributions from the wall can be given after streaming step.

The specified boundary conditions are decided by the combination parameters. The combination parameters for gaseous microflow are decided by $Kn$ because the gaseous slip should be attributed to the rarefaction effects (Knudsen number $Kn$) [20, 28]. However, the liquid slip is mainly controlled by the characteristic of the wall [10, 11].

There are two obstacles for applying these schemes to simulate liquid microflow. One is that the HDSR, HDBB, MDSR, MDBB schemes can only obtain a limited range of slip length [20, 28]. The other one is that the combination parameters for liquid slip should be specified with the slip length but not $Kn$. We will solve these problems in the next subsection.

### *2.3. Analysis of slip boundary conditions for simulation of liquid flow*

In this subsection, through theoretical analysis, these slip boundary conditions are introduced from gas flow to simulate liquid slip. We propose a method to specify the combination parameters with the slip length instead of the Knudsen number. Researchers have studied the numerical stability of the slip boundary conditions for gas flow [20, 28]. The numerical stability and the accuracy of these boundary conditions for liquid flow are consistent with gas flow in nature [36]. It can be concluded from the following simulations that the numerical stability and the accuracy of the improved slip boundary conditions for liquid flow are not worse than gas flow.

#### *2.3.1. Basic assumptions of unidirectional steady liquid flow*

It is difficult to analyse the slip boundary conditions in complex flows. So some basic assumptions should be given. Guo et al. [20] and Tao et al. [38] adopted the unidirectional steady gas flow to obtain the relations between the combinations parameters and the Knudsen number. Results show that the relations are accurate and reliable enough to simulate complex gas flows with slip boundary condition. Wang [36] used the unidirectional liquid flow to deduce the relation between the combination parameter of BSR scheme and the slip length. Simulations demonstrate that the relation is suitable even for unsteady Womersly flow with liquid slip boundary condition. In the following analysis, for simplicity, we also consider a unidirectional liquid flow as shown in Fig.1 and 2. The assumptions are expressed as:

$$\rho = const, \qquad u_y = 0, \qquad a_y = 0, \qquad \frac{\partial \phi}{\partial x} = 0, \qquad \frac{\partial \phi}{\partial t} = 0 \tag{14}$$

where $\phi$ represents an arbitrary flow variable, $u_y$ is the $y$ component of the velocity, $a_y$ is the $y$ component of the body force $\vec{a}$.

According to Eq.(6), the velocities at place $j$ can be calculated by

$$\rho u_j = c(f_1^j - f_3^j + f_5^j - f_6^j + f_8^j - f_7^j) + \frac{\Delta t}{2}\rho a \tag{15}$$

where $f_i^j$ means the distribution function at place $j$ and velocity $\vec{e}_i$, and $a$ is the $x$ component of the acceleration $\vec{a}$.

The unidirectional property of this flow suggests that

$$f_1^j - f_3^j = \bar{f}_1^j - \bar{f}_3^j \tag{16}$$

Considering the streaming rules Eq.(4) and these above assumptions, we have

$$f_5^2 - f_6^2 = \bar{f}_5^1 - \bar{f}_6^1, \qquad f_8^1 - f_7^1 = \bar{f}_8^2 - \bar{f}_7^2 \tag{17}$$

*2.3.2. Improvement for four of these slip boundary conditions*

With Eqs.(3), (5), (15), (16), (17) at hand and following the procedures of Guo [20], we can derive the relation between $u_1$ and $u_2$, where $u_j$ denotes the velocity at location $j$ in Fig.1. For the HBSR scheme, we obtain

$$u_2 = \frac{1-2\tau+2r(\tau-2)}{1-2\tau+2r(\tau-1)}u_1 + \frac{6(2\tau-1)+r(8\tau^2-20\tau+11)}{(2\tau-1)[1-2\tau+2r(\tau-1)]}\Delta t a \tag{18}$$

For the HDSR scheme, we get

$$u_2 = \frac{1-2\tau+q(\tau-2)}{1-2\tau+q(\tau-1)}u_1 + \frac{6(2\tau-1)+0.5q(8\tau^2-20\tau+11)}{(2\tau-1)[1-2\tau+q(\tau-1)]}\Delta t a \tag{19}$$

For the HDBB scheme, we have

$$u_2 = \frac{1-2\tau+(2-s)(\tau-2)}{1-2\tau+(2-s)(\tau-1)}u_1 + \frac{6(2\tau-1)+0.5(2-s)(8\tau^2-20\tau+11)}{(2\tau-1)[1-2\tau+(2-s)(\tau-1)]}\Delta t a \tag{20}$$

It is observed that if we set $q = 2r$, Eqs.(18) and (19) are identical, which means that the HBSR and HDSR schemes are equivalent. It agrees well with the conclusion of Guo [20]. Guo [20] also found that if $r = 0.5$, the HBSR scheme can realize the discrete full diffuse boundary condition ($q = 1$), which means the HBSR scheme with $r = 0.5$ is equivalent to the discrete full diffuse boundary condition.

Similarly, if we set $s = 2 - 2r$, Eqs.(18) and (20) are identical. Following the procedure of Guo [20], it is also proved that the HBSR scheme with $r = 0.5$ is equivalent to the discrete full diffuse boundary condition.

Based on this equivalence, we can have the following derivation:

$$\begin{cases} f_2^{eq} \\ f_5^{eq} \\ f_6^{eq} \end{cases} \Longleftrightarrow \begin{cases} \bar{f}_4 \\ 0.5\bar{f}_7 + 0.5\bar{f}_8 \\ 0.5\bar{f}_8 + 0.5\bar{f}_7 \end{cases}$$

So the HDSR scheme can be equivalent to the following relations:

$$\begin{cases} qf_2^{eq} + (1-q)\bar{f}_4 \\ qf_5^{eq} + (1-q)\bar{f}_8 \\ qf_6^{eq} + (1-q)\bar{f}_7 \end{cases} \Longleftrightarrow$$

$$\begin{cases} q\bar{f}_4 + (1-q)\bar{f}_4 \\ q(0.5\bar{f}_7 + 0.5\bar{f}_8) + (1-q)\bar{f}_8 \\ q(0.5\bar{f}_7 + 0.5\bar{f}_8) + (1-q)\bar{f}_7 \end{cases}$$

$$\Longleftrightarrow \begin{cases} \bar{f}_4 \\ 0.5q\bar{f}_7 + (1-0.5q)\bar{f}_8 \\ 0.5q\bar{f}_8 + (1-0.5q)\bar{f}_7 \end{cases}$$

The conventional HDSR scheme assumes that the two extreme cases of the interaction between molecules and walls are the discrete full diffusive and the specular reflection boundary conditions [26], and the conventional HDBB scheme assumes that the two extreme cases are the discrete fully diffusive and the bounce back boundary conditions [28]. Therefore, for the conventional HDSR and HDBB schemes, the combination parameters are limited to [0, 1].

For actual liquid flow, velocity slip may range from no slip to nearly full slip. Comparing the equivalence form of the HDSR scheme with Eq.(8), we can find $r = 0.5q$. For $r$ varies from 0 to 1, we can naturally obtain that $0 \leq q \leq 2$. The numerical results below also prove our improvements. Similarly, the combination parameters of the HDBB, MDSR and MDBB schemes can be expanded from [0,1] to [0,2]. In the physical sense, these schemes are improved based on the equivalence to the BSR scheme, and the two extreme cases of the interaction between molecules and walls change to the bounce back and the specular reflection boundary conditions.

Our improvement has three advantages comparing with the conventional schemes. The first one is that it can realize a wider range of velocity slip. The second one is that we make it possible to apply these schemes to simulate liquid flow. The third one is that the HDBB and MDBB schemes have the potential to simulate liquid flow with complex geometries for their local computations.

In order to simulate specified velocity slip of liquid flow, we still need to relate the slip length to the combination parameters.

*2.3.3. Relating slip length to the combination parameters*

For liquid flow, Navier's slip model has been accepted by many researchers [14], having the form of

$$u_s = b\frac{\partial u}{\partial \vec{n}}|_{wall} \tag{21}$$

where $u_s$ is the slip velocity at the wall, $b$ is the slip length, and $\frac{\partial u}{\partial \vec{n}}$ means the velocity gradient in the normal direction of the wall.

The slip length can quantify the velocity slip of liquid flow and can be measured by experiment [17]. In order to get a specified boundary condition for liquid micro-flow, we adopt a widely used linear slip model, the Navier's slip model, as the base to deduce the relationships between the slip length and the combination parameters of the formerly discussed slip boundary conditions.

Firstly, we analyse three half-way schemes: Eqs.(8), (9) and (10). Wang et al. [36] adopted the Couette flow with linear velocity gradient to deduce the relation between the combination parameters of BSR scheme with the slip length. Results show that the relations they obtained are accurate and reliable enough even for unsteady nonlinear flow. So we also take the Couette flow in the following derivation.

For the Couette flow (linear velocity gradient, $a = 0$), the equation can be written as

$$u = \beta y + u_s \tag{22}$$

where $\beta$ is a parameter, $y$ is the distance from bottom wall and $u_s$ is the slip velocity at the wall.

Substituting $u_1$ and $u_2$ of the Couette flow into Eqs.(18), (19), (20) respectively, we can get the relations between the slip velocity and the combination parameters of the half-way schemes:

$$u_s = \begin{cases} \beta\frac{(1-r)(2\tau-1)}{2r} \\ \beta\frac{(1-\frac{q}{2})(2\tau-1)}{q} \\ \beta\frac{\frac{s}{2}(2\tau-1)}{2-s} \end{cases} \tag{23}$$

Based on Eqs.(21) and (23), we can deduce the relations between the slip length and the combination parameters of the half-way schemes:

$$b = \begin{cases} \frac{(1-r)(2\tau-1)}{2r} \\ \frac{(1-\frac{q}{2})(2\tau-1)}{q} \\ \frac{\frac{s}{2}(2\tau-1)}{2-s} \end{cases} \tag{24}$$

From Eq.(24), we can obtain the relations between the combination parameters and the slip length:

$$\begin{cases} r = \frac{1}{1+\frac{2b}{2\tau-1}} \\ q = \frac{2}{1+\frac{2b}{2\tau-1}} \\ s = \frac{2}{1+\frac{2\tau-1}{2b}} \end{cases} \tag{25}$$

Eq.(24) shows that the slip length is decided by the combination parameter and relaxation time. It can be seen from Eq.(24) that with a wider range of $q$ and $s$ ($[0,\ 2]$), the range of the slip length that the HDSR and HDBB schemes can simulate is also larger.

It can be noted from Eq.(25) that there is no discrete lattice effect for linear flow and the combination parameters can be specified by given slip length and the relaxation time.

For more general flow, there may be discrete effects caused by different lattice numbers. We will analyse the discrete effects of the slip boundary conditions with the case of the Poiseuille flow below.

For the Poiseuille flow (non-linear velocity gradient, $a \neq 0$), the equation is

$$u = \frac{a}{2\nu} y(H - y) + u_s \tag{26}$$

where $H$ is the gap between two fixed plates.

Substituting Eq.(26) into Eqs.(18), (19), (20) respectively, we find that the slip velocity is determined by

$$u_s = \begin{cases} \frac{aH}{2\nu}\frac{(1-r)(2\tau-1)}{2r} + \frac{aH}{2\nu}\frac{(2\tau-1)^2-3/4}{3H} \\ \frac{aH}{2\nu}\frac{(1-\frac{q}{2})(2\tau-1)}{q} + \frac{aH}{2\nu}\frac{(2\tau-1)^2-3/4}{3H} \\ \frac{aH}{2\nu}\frac{\frac{s}{2}(2\tau-1)}{2-s} + \frac{aH}{2\nu}\frac{(2\tau-1)^2-3/4}{3H} \end{cases} \tag{27}$$

for the Poiseuille flow.

Combining Eq.(21) and Eq.(27), we can find the slip length is determined by

$$b = \begin{cases} \frac{(1-r)(2\tau-1)}{2r} + \frac{(2\tau-1)^2-3/4}{3H} \\ \frac{(1-\frac{q}{2})(2\tau-1)}{q} + \frac{(2\tau-1)^2-3/4}{3H} \\ \frac{\frac{s}{2}(2\tau-1)}{2-s} + \frac{(2\tau-1)^2-3/4}{3H} \end{cases} \tag{28}$$

for the Poiseuille flow.

From Eq.(28), we can obtain the relations between the combination parameters and the slip length:

$$\begin{cases} r = \frac{1}{1+\frac{2b-2(2\tau-1)^2/(3H)+1/(2H)}{2\tau-1}} \\ q = \frac{2}{1+\frac{2b-2(2\tau-1)^2/(3H)+1/(2H)}{2\tau-1}} \\ s = \frac{2}{1+\frac{2\tau-1}{2b-2(2\tau-1)^2/(3H)+1/(2H)}} \end{cases} \tag{29}$$

for the Poiseuille flow.

For the Poiseuille flow, it is observed from Eq.(28) that the slip length is influenced by two parts: a physical part depending on the combination parameter and relaxation time, and a numerical part depending on the relaxation time and the value of $H$ related to the grid size. If we set $r = \frac{q}{2} = 1 - \frac{s}{2} = 1$, the half-way scheme equals to the pure half-way bounce-back scheme. According to Eq.(28), this pure half-way bounce-back scheme generates a nonzero slip length, due to the discrete effect. Moreover, it also shows that all of the three half-way schemes can not be applied to the Poiseuille flow with $b < \frac{(2\tau-1)^2-3/4}{3H}$ when $0 \leq 2r, q, s \leq 2$. The relative error of the slip length caused by the discrete effect can be quantified by

$$L_{error} = \frac{(2\tau-1)^2 - 3/4}{3bH} \tag{30}$$

In order to obtain an accurate boundary condition for liquid flow, the discrete effects should be corrected or reduced greatly. For the Poiseuille flow, the discrete error can be analysed and calculated. So we can consider the influence of the discrete effect on the slip length when calculating the combination parameters, as what has been done in Eq.(29). In this way, the discrete effects can be corrected and we can simulate the slip length accurately.

But for general flow without known equations, it is difficult to obtain the equation of discrete effect part. So we can not consider the influence of the discrete effect on the slip length when calculating the combination parameters. Even though we cannot eliminate the discrete effect completely, we still have other ways to reduce the discrete effects. The discrete effect is controlled by the relaxation time and the lattice numbers $H$. One way is to adjust the relaxation time. If a suitable $\tau$ is given, the relative error can be reduced greatly. But a fixed $\tau$ will bring much inconvenience to the choice of the grid size and the characteristic velocity in the lattice Boltzmann

simulation. The other way is to refine lattice. Increasing $H$ will greatly reduce the error. Moreover, in order to ensure $0 \leq 2r, q, s \leq 2$, $b$ should be no smaller than $\frac{(2\tau-1)^2-3/4}{3H}$ for the half-way schemes. If $H$ is big enough, the range of the simulated slip length will be expanded and Eq.(28) will recover to Eq.(24). So refining lattice is necessary and effective to reduce the discrete effects for the lattice Boltzmann simulation of liquid slip flow. With refining grids, Eq.(29) for the Poiseuille flow will recover to Eq.(25) for the Couette flow and the general flow can be simulated with Eq.(25) of the half-way schemes.

Similarly to the analysis of the half-way schemes, the slip length in the modified schemes is decided by

$$b = \begin{cases} \frac{\tau(1-\bar{r})}{\bar{r}} \\ \frac{\tau(2-\bar{q})}{\bar{q}} \\ \frac{\tau\bar{s}}{2-\bar{s}} \end{cases} \tag{31}$$

for the linear liquid flow, and

$$b = \begin{cases} \frac{\tau(1-\bar{r})}{\bar{r}} + \frac{8\tau^2-2\tau-1}{6H} \\ \frac{\tau(2-\bar{q})}{\bar{q}} + \frac{8\tau^2-2\tau-1}{6H} \\ \frac{\tau\bar{s}}{2-\bar{s}} + \frac{8\tau^2-2\tau-1}{6H} \end{cases} \tag{32}$$

for the Poiseuille flow.

The combination parameters for the modified schemes are given by

$$\begin{cases} \bar{r} = \frac{1}{1+\frac{b}{\tau}} \\ \bar{q} = \frac{2}{1+\frac{b}{\tau}} \\ \bar{s} = \frac{2}{1+\frac{\tau}{b}} \end{cases} \tag{33}$$

for the linear liquid flow, and

$$\begin{cases} \bar{r} = \frac{1}{1+\frac{b-(8\tau^2-2\tau-1)/(6H)}{\tau}} \\ \bar{q} = \frac{2}{1+\frac{b-(8\tau^2-2\tau-1)/(6H)}{\tau}} \\ \bar{s} = \frac{2}{1+\frac{\tau}{b-(8\tau^2-2\tau-1)/(6H)}} \end{cases} \tag{34}$$

for the Poiseuille flow.

For the Poiseuille flow, with $0 \leq 2\bar{r}, \bar{q}, \bar{s} \leq 2$, the smallest simulated slip length is $\frac{8\tau^2-2\tau-1}{6H}$. The modified schemes with Eq.(34) are incapable

of simulating the Poiseuille flow with $b < \frac{8\tau^2-2\tau-1}{6H}$ when $0 \leq 2\bar{r}, \bar{q}, \bar{s} \leq 2$. But increasing $H$ can help expand the simulated slip length and reduce the discrete effects. If $H$ is large enough, Eq.(32) for the Poiseuille flow will recover to Eq.(31) for the linear flow and Eq.(34) for the Poiseuille flow will recover to Eq.(33) for the linear flow. So it is reasonable to simulate more general flows with Eq.(33) of the modified schemes.

For more general cases, it is difficult to deduce the exact functions between the combination parameters and the slip length. Some researchers used the Poiseuille flow to approximate the actual flow near the wall [37, 38, 40, 41]. In fact, if the grid is fine enough, the discrete effects can be ignorable and the local flow at the wall can be approximated as flow with linear velocity gradient [36]. It is also proved by the numerical results below. The Eq.(25) of the half-way schemes and Eq.(33) of the modified schemes are deduced based on the flow with linear velocity gradient.

With Eq.(25) of the half-way schemes, we have

$$\begin{cases} f_2 = \bar{f}_4 \\ f_5 = \frac{1}{1+\frac{2b}{2\tau-1}}\bar{f}_7 + (1 - \frac{1}{1+\frac{2b}{2\tau-1}})\bar{f}_8 \\ f_6 = \frac{1}{1+\frac{2b}{2\tau-1}}\bar{f}_8 + (1 - \frac{1}{1+\frac{2b}{2\tau-1}})\bar{f}_7 \end{cases} \tag{35}$$

for the HBSR scheme;

$$\begin{cases} f_2 = \frac{2}{1+\frac{2b}{2\tau-1}}f_2^{eq} + (1 - \frac{2}{1+\frac{2b}{2\tau-1}})\bar{f}_4 \\ f_5 = \frac{2}{1+\frac{2b}{2\tau-1}}f_5^{eq} + (1 - \frac{2}{1+\frac{2b}{2\tau-1}})\bar{f}_8 \\ f_6 = \frac{2}{1+\frac{2b}{2\tau-1}}f_6^{eq} + (1 - \frac{2}{1+\frac{2b}{2\tau-1}})\bar{f}_7 \end{cases} \tag{36}$$

for the HDSR scheme;

$$\begin{cases} f_2 = \frac{2}{1+\frac{2\tau-1}{2b}}f_2^{eq} + (1 - \frac{2}{1+\frac{2\tau-1}{2b}})\bar{f}_4 \\ f_5 = \frac{2}{1+\frac{2\tau-1}{2b}}f_5^{eq} + (1 - \frac{2}{1+\frac{2\tau-1}{2b}})\bar{f}_7 \\ f_6 = \frac{2}{1+\frac{2\tau-1}{2b}}f_6^{eq} + (1 - \frac{2}{1+\frac{2\tau-1}{2b}})\bar{f}_8 \end{cases} \tag{37}$$

for the HDBB scheme.

With Eq.(33) of the modified schemes, we obtain

$$\begin{cases} f_2 = f_4 \\ f_5 = \frac{1}{1+\frac{b}{\tau}}f_7 + (1 - \frac{1}{1+\frac{b}{\tau}})f_8 \\ f_6 = \frac{1}{1+\frac{b}{\tau}}f_8 + (1 - \frac{1}{1+\frac{b}{\tau}})f_7 \end{cases} \tag{38}$$

for the MBSR scheme;

$$\begin{cases} f_2 = \frac{2}{1+\frac{b}{\tau}} f_2^{eq} + (1 - \frac{2}{1+\frac{b}{\tau}}) f_4 \\ f_5 = \frac{2}{1+\frac{b}{\tau}} f_5^{eq} + (1 - \frac{2}{1+\frac{b}{\tau}}) f_8 \\ f_6 = \frac{2}{1+\frac{b}{\tau}} f_6^{eq} + (1 - \frac{2}{1+\frac{b}{\tau}}) f_7 \end{cases} \tag{39}$$

for the MDSR scheme;

$$\begin{cases} f_2 = \frac{2}{1+\frac{\tau}{b}} f_2^{eq} + (1 - \frac{2}{1+\frac{\tau}{b}}) f_4 \\ f_5 = \frac{2}{1+\frac{\tau}{b}} f_5^{eq} + (1 - \frac{2}{1+\frac{\tau}{b}}) f_7 \\ f_6 = \frac{2}{1+\frac{\tau}{b}} f_6^{eq} + (1 - \frac{2}{1+\frac{\tau}{b}}) f_8 \end{cases} \tag{40}$$

for the MDBB scheme.

The slip boundary conditions (Eq.(35) to (40)) are designed to simulate the general liquid flow with slip velocity. The above analysis shows that the Eq.(29) of the half-way schemes and the Eq.(34) of the modified schemes depend on the model of the Poiseuille flow. For the Eq.(29), the smallest simulated slip length is $\frac{(2\tau-1)^2-3/4}{3H}$. For the Eq.(34), the smallest simulated slip length is $\frac{8\tau^2-2\tau-1}{6H}$. For the slip boundary conditions (Eq.(35) to (40)), with refining grids, the discrete effects are ignorable and the simulated smallest slip length is extremely close to zero. Among these slip boundary conditions, the specular reflection parts of the HBSR, MBSR, HDSR and MDSR are not computed locally, making it difficult to use these four schemes for curved boundaries [38]. On the contrary, the HDBB Scheme Eq.(37) and the MDBB scheme Eq.(40) are suitable for the simulation of liquid flows with complex geometries for the nature of their local computations.

## 3. Numerical validation and discussion

In the above section, the slip boundary conditions are introduced for liquid micro-flow. The combination parameters of the HDSR, MDSR, HDBB, and MDBB schemes are expanded from [0,1] to [0,2]. The relations between the combination parameters and the slip length are deduced theoretically.

In this section, the proposed slip boundary conditions are tested carefully through these cases: the plane Couette flow, the Poiseuille flow, the unsteady Womersley flow, the channel flow with constant inlet velocity and the cylindrical Couette flow.

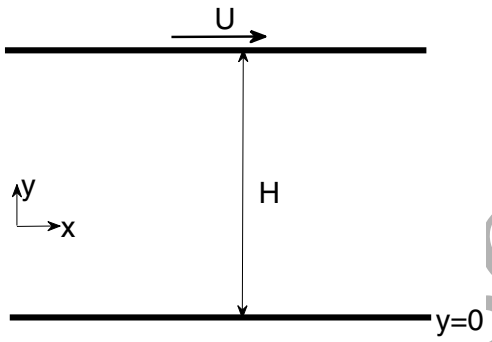


Figure 3: Schematic of the 2D Couette flow

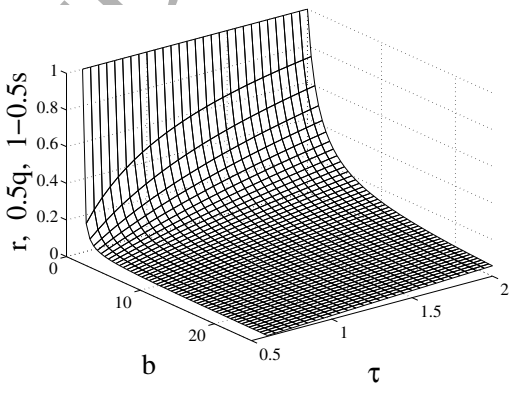


Figure 4: Dependence of the combination parameter on $b$ and $\tau$ for the half-way schemes

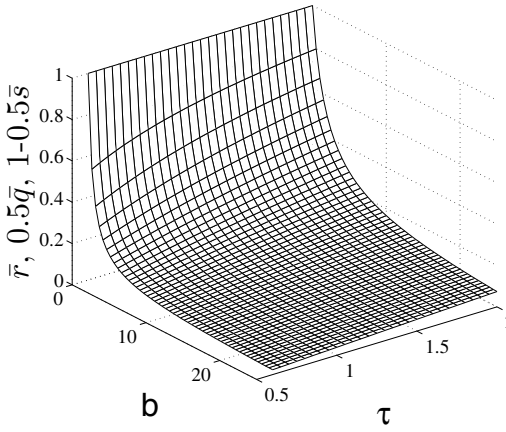


Figure 5: Dependence of the combination parameter on $b$ and $\tau$ for the modified schemes

### *3.1. Plane Couette flow with slip boundary*

A plane Couette flow model is used to validate the slip boundary conditions for linear flow. The sketch of this liquid flow is shown in Fig.3. Simulations are performed with a gap $H = 32$. The upper plate is given a constant speed $U = 0.01$ with no-slip boundary condition. Slip boundary condition is employed for the still bottom plate. The combination parameters of the slip boundary conditions are determined by predefined slip length through Eq.(25) and Eq.(33). The periodic boundary conditions are applied to the inlet and outlet. Grid independence has been verified by cases with different length of plate. For the following simulations, the length of plate $L = 32$ is adopted. All variables are in lattice units if there is no special mention. With these given boundary conditions and the linear slip model, Eq.(22) of the Couette flow can rewritten as

$$u = \frac{y}{H+b}U + \frac{b}{H+b}U \tag{41}$$

At first, we examine the relative error between the predefined slip length and the slip length produced by each slip condition when simulating this plane Couette liquid flow. Without losing generality, $\tau$ is set from 0.6 to 2 and the predefined slip length varies from 0 to 25. Fig.4 and Fig.5 depict the combination parameters as a function of the given slip length and the relaxation time for the half-way schemes and the modified schemes respectively. Since the three half-way schemes are equivalent and produce nearly the same

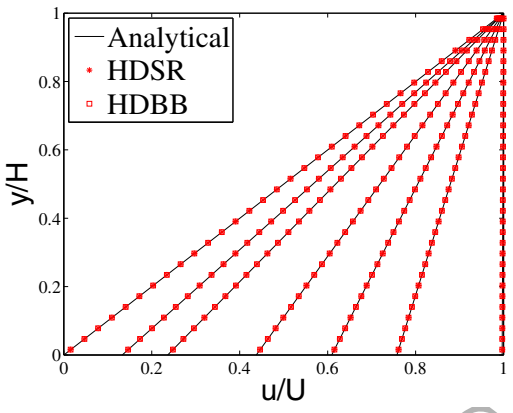


Figure 6: Velocity distribution of the Couette flow for $q = 2 - s$ =2, 0.04, 0.02, 0.008, 0.004, 0.002, 0.00002 (from the leftmost line to the rightmost line).

results here, we only display one set of data in Fig.4. For the same reason, we also do this for the modified schemes in Fig.5. Totally 1152 individual simulations are conducted to test the slip boundary conditions. Results show that the relative errors between input slip lengths and corresponding output slip lengths are nearly zero.

Then, we test the performance of the combination parameters of the HDSR, MDSR, HDBB and MDBB schemes within the range of [0, 2]. $\tau = 0.6$ is used here. Besides, we set $q = 2-s = 2, 0.04, 0.02, 0.008, 0.004, 0.002, 0.00002$, and $\bar{q} = 2 - \bar{s} = 2, 0.2, 0.08, 0.04, 0.02, 0.008, 0.00002$. The simulated velocities for different combination parameters are shown in Fig.6 for the HDSR and HDBB schemes, and Fig.7 for the MDSR and MDBB schemes. Numerical results are in excellent agreement with the analytical results given by Eq.(41). Fig.6 and Fig.7 also show that slip lengths change slowly with $0.2 < q, \bar{q}, 2 - s, 2 - \bar{s} \leq 2$ but rapidly with $0 < q, \bar{q}, 2 - s, 2 - \bar{s} < 0.2$. It is consistent with the conclusion obtained from Fig.4 and Fig.5.

In addition, discrete effects in the slip boundary conditions are examined in linear liquid flow. Simulations are carried out with H=32, 8, 4, respectively. $\tau$ is set as 0.6. The simulated velocities obtained by three half-way schemes are almost exactly the same for the same case. So we use one set of data named 'Half-way' in Fig.8 to represent the results of all three half-way schemes. Similarly, the results of three modified schemes are shown as one set of data named 'Modified'. As shown in Fig.8, the numerical results are in excellent agreement with the analytical results given by Eq.(41) for b/H=0,

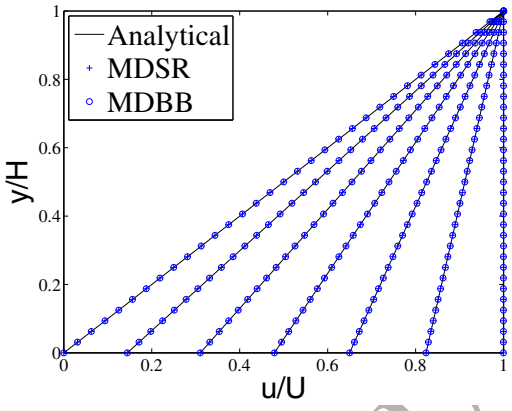


Figure 7: Velocity distribution of the Couette flow for $\bar{q} = 2 - \bar{s}$ =2, 0.2, 0.08, 0.04, 0.02, 0.008, 0.00002 (from the leftmost line to the rightmost line)

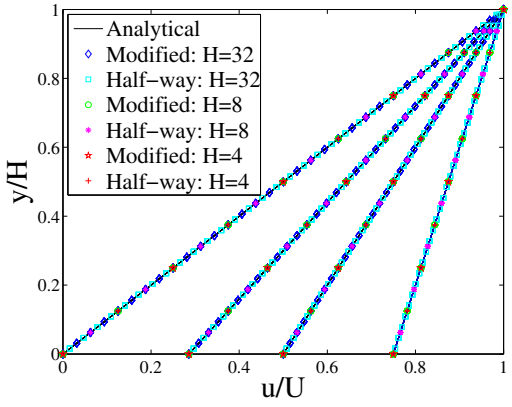


Figure 8: Velocity distribution of the Couette flow for $b/H$ =0, 0.4, 1, 3 (from the leftmost line to the rightmost line).

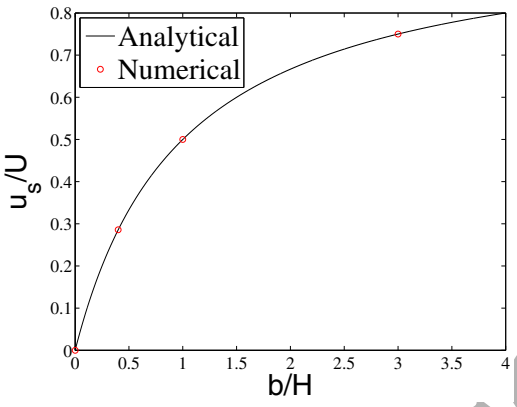


Figure 9: Slip velocity of the Couette flow for different dimensionless slip length.

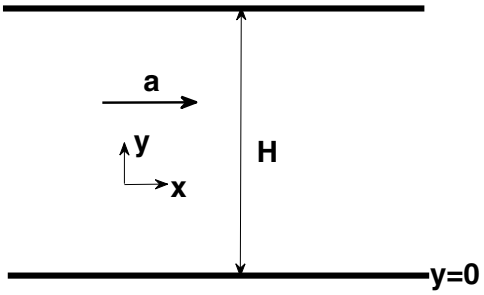


Figure 10: Model of the Poiseuille flow ($a$: a constant acceleration)

0.4, 1 and 3. It is noticed that the simulated velocities are still accurate enough even in cases with only four lattices. There is nearly no discrete effect in the proposed slip boundary conditions for linear liquid flow. This agrees well with Eqs.(24) and (31). The dimensionless slip velocities of the Couette flow for b/H=0, 0.4, 1 and 3 are depicted in Fig.9. Excellent agreement can be found between the numerical results and the analytical solutions given by Eq.(41).

### *3.2. Poiseuille flow with slip boundary*

Poiseuille flow is simulated to test the slip boundary conditions for non-linear liquid flow. As shown in Fig.10, the gap between two still plates is

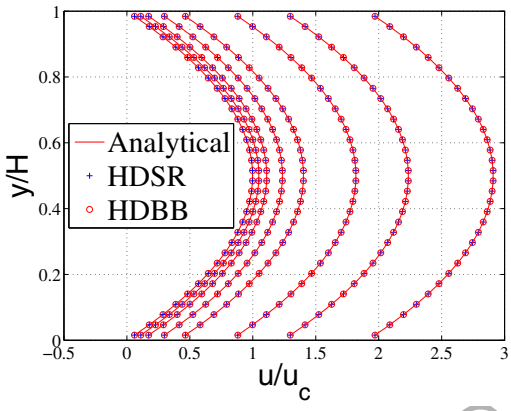


Figure 11: Velocity profiles of the Poiseuille flow for $q = 2 - s$ =2, 0.4, 0.2, 0.1, 0.06, 0.03, 0.02, 0.013 (from the leftmost curve to the rightmost curve).

$H = 32$. The flow is driven by a constant body force $a = 10^{-5}$. The inlet and outlet of the channel employ the periodic boundary conditions. The length of the channel is set as 32. Combining Eqs.(21) and (26), the analytical velocity profiles of the Poiseuille flow can be expressed as

$$u(y) = -\frac{a}{2\nu}y^2 + \frac{aH}{2\nu}y + \frac{aH}{2\nu}b$$

With the characteristic speed $u_c = aH^2/8\nu$, the above equation can be rewritten as

$$U(y) = \frac{u(y)}{u_c} = 4\frac{y}{H}(1 - \frac{y}{H}) + 4\frac{b}{H} \tag{42}$$

We examine the improved HDSR, HDBB, MDSR and MDBB schemes for the Poiseuille flow with $\tau = 0.6$ ($\nu = 1/30$). Here, we set $q = 2 - s = 2$, 0.4, 0.2, 0.1, 0.06, 0.03, 0.02, 0.013, and $\bar{q} = 2 - \bar{s} = 2$, 1.2, 0.6, 0.4, 0.2, 0.15, 0.10, 0.07, 0.05. The simulated velocities are depicted in Fig.11 for the half-way schemes and Fig.12 for the modified schemes. Clearly, these four improved schemes can ensure the accuracy and reliability of the lattice Boltzmann simulation of the Poiseuille flow with slip boundary. It is noted that the distances between two adjacent velocity profiles along the horizontal direction in Fig.11 and Fig.12 are the same. This phenomenon can be explained by Eq.(42). For the same $a$, $H$, $\nu$ and $y$, the first part of Eq.(42) is constant, and the second part is only decided by $b$. Fig.11 and Fig.12 also indicate that the slip velocities at two still plates become larger when $q, 2 - s, \bar{q}, 2 - \bar{s}$

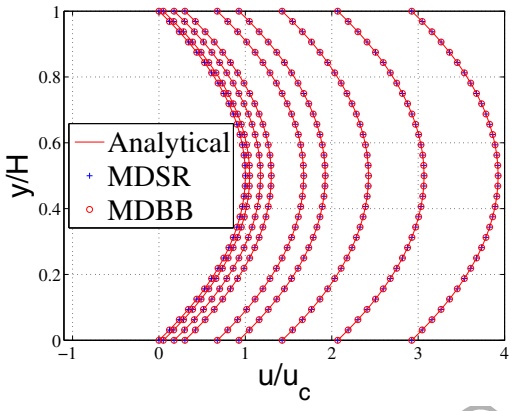


Figure 12: Velocities profiles of the Poiseuille flow for $\bar{q} = 2 - \bar{s}$ =2, 1.2, 0.6, 0.4, 0.2, 0.15, 0.10, 0.07, 0.05 (from the leftmost curve to the rightmost curve).

become smaller. It is consistent with the analytical results of Eqs.(28) and (32).

Discrete effects of the slip boundaries for the Poiseuille flow are also studied. Considering the discrete effects, the combination parameters are calculated by predefined slip length according to Eqs.(29) and (34). Simulations will diverge if the predefined slip length is smaller than a specific value. It can be explained by Eqs.(29) and (34). We define these specific values as the smallest simulated slip lengths ($b_s$). If $b < b_s$, the combination parameters will be out of the range of [0,2] and these slip boundary conditions are not effective any more. $b_s * H$ as a function of $\tau$ are depicted in Fig.13. It is observed from Fig.13 that the smallest simulated slip lengths of the half-way schemes are smaller than the modified schemes for cases with the same $H$ and $\tau$. So if $H$ and $\tau$ are given, the half-way schemes can simulate a wider range of slip length than the modified schemes. If $\tau \leq \frac{\sqrt{3}}{4} + \frac{1}{2}$, the half-way schemes can be applied to liquid flow with slip length from zero to infinite. In this sense, the half-way schemes are better choices than the modified schemes for the Poiseuille flow. Fig.13 also shows that larger $H$ is beneficial to obtain a wider range of simulated slip length with the same $\tau$.

Discrete effects have influence not only on the application scope of the slip boundary conditions, but also on the accuracy and reliability of simulations. To examine the discrete effects of the slip boundary conditions, simulations are carried out with $\tau = 2$, $b/H = 0.5$ and $H$ =4, 8 and 64. The combination parameters are calculated by Eqs.(25) and (33). It is because that the

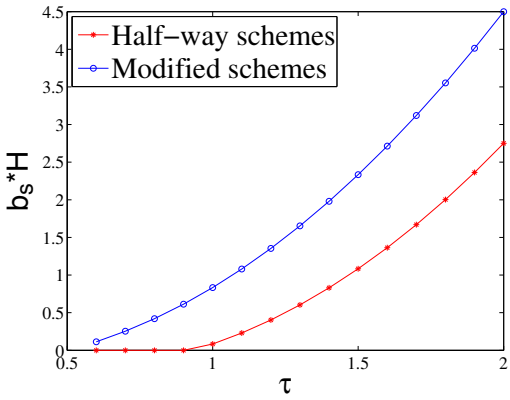


Figure 13: Smallest simulated slip length varies with the relaxation time for the Poiseuille flow.

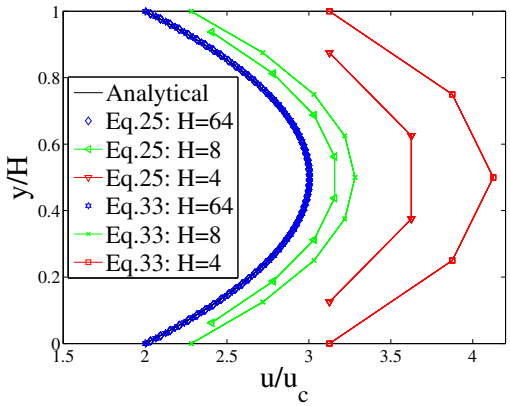


Figure 14: Velocity profiles of the Poiseuille flow with $b/H$=0.5.

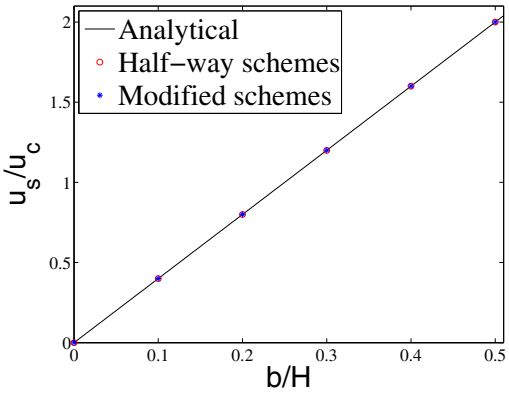


Figure 15: Slip velocity of the Poiseuille flow for different dimensionless slip length.

parts with $H$ in Eq.(29) and Eq.(34) can be neglected if $H$ is large enough. Then Eq.(29) will recover to Eq.(25) and Eq.(34) will recover to (33). The simulation results are depicted in Fig.14. It is clear that the discrete effects have great influence on slip velocities if the lattice number is not enough. The velocity profiles simulated with Eqs.(25) and (33) are closer to the analytical solution with larger $H$. When $H = 64$, the numerical results are almost the same as the analytical solution. So grid refinement is meaningful and effective for decreasing discrete effects. Besides, for the same $H$, velocity distributions simulated with Eq.(25) (Half-way schemes) are closer to the analytical results than Eq.(33) (modified schemes) in Fig.14. The discrete effects have less influence on the results of the half-way schemes than that of the modified schemes. From this point, the half-way schemes have more advantage than the modified schemes. We also conduct the simulations of Poiseuille flow with $b/H$ =0.1, 0.2, 0.3, 0.4. $H$ is set as 64. The slip velocities at the wall of the Poiseuille flow are depicted as the function of dimensionless slip length in Fig.15. It can be observed that the numerical results obtained by the half-way schemes Eq.(25) and the modified schemes Eq.(33) are in good agreement with the analytical solutions predicted by Eq.(42).

The results obtained by Eq.(25) and Eq.(33) also indicate the possibility of simulating complex flows with fine enough grid. We will explore this direction in the next subsection.

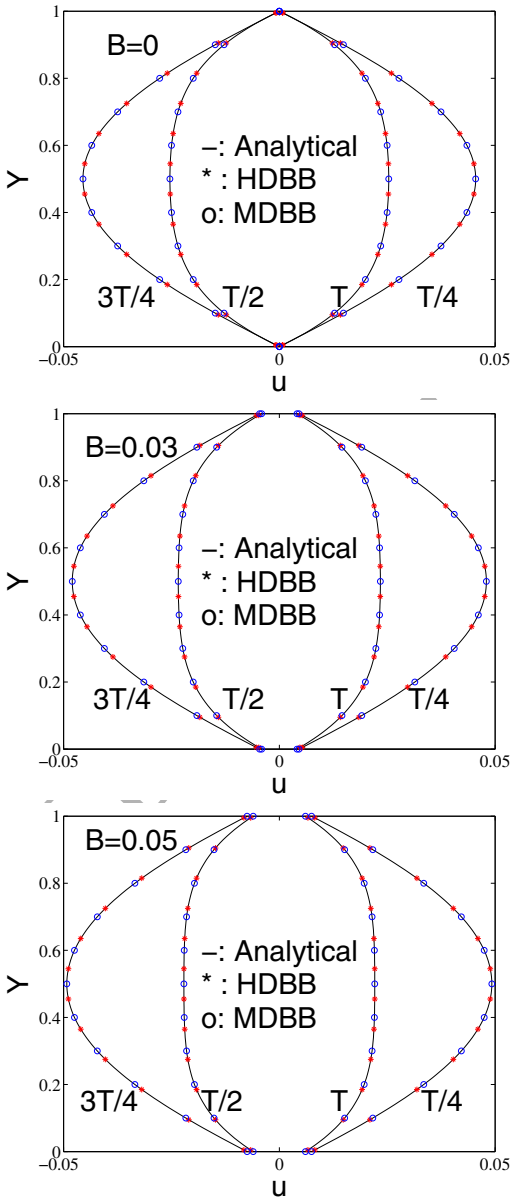


Figure 16: Velocity profiles of the Womersley flow ( $B$ =0, 0.03 and 0.05 respectively from the top to the bottom ).

### 3.3. Unsteady Womersley flow with slip boundary

Although the improved slip boundary conditions are validated by the simulation of the Couette flow and the Poiseuille flow in the above subsections, the generality of our improved slip boundary conditions for simulating complex flow still needs to be verified. In this subsection, we simulate the Womersley flow, which is unsteady and strongly nonlinear. And the direction of the velocity may be different at different time. The model of the Womersley flow is similar to the Poiseuille flow in Fig.10, except that the constant acceleration $a$ is replaced by a periodic one $a(t)$. In this simulation, we set $a(t) = a_m cos(\omega t)$, where $a_m$ is the amplitude and $\omega$ is the frequency. The frequency is related to the period of the acceleration by $\omega = \frac{2\pi}{T}$. The analytical solution of the Womersley flow with slip boundary condition can be expressed as [36]

$$u(y) = Real[i\frac{a_m}{\omega}(1 - \frac{cos(2\lambda Y - \lambda)}{cos\lambda - 2B\lambda sin\lambda})e^{i\omega t}] \tag{43}$$

where $i$ is the symbol of imaginary number and *Real* is the real part. Besides, $Y$ is the dimensionless form of $y$ with $Y = y/H$ and $B$ is the dimensionless form of the slip length $b$ with $B = b/H$. The parameter $\lambda$ is defined as

$$\lambda^2 = -iW_0^2, W_0^2 = \frac{\omega H^2}{4\nu} \tag{44}$$

where $W_0$ is the Womersley number.

In this simulation, we take the improved DBB schemes to simulate the liquid slip at the wall. Wang et al. [36] tested the BSR schemes with $H = 100$ in the simulation of the unsteady Womersley flow, and found that H=100 is find enough for this problem to obtain accurate and reliable results. So we also use $H = 100$. The kinematic viscosity is set as 0.001 and the Womersley number is set as 2.0. The Reynolds number is defined as $Re = u_m H/\nu$, where $u_m$ is calculated by $u_m = \frac{a_m H^2}{8\nu}$. We simulate the case with $Re = 10000$ to test the improved DBB schemes. The combination parameters are given according to Eq.(25) and Eq.(33) for $B$ =0, 0.03, 0.05. The velocity profiles of one period are presented in Fig.16. The numerical results obtained by the HDBB and MDBB schemes are in excellent agreements with the analytical solutions given by Eq.(43). It can be observed that the velocity profiles at $T$, $T/4$, $T/2$ and $3T/4$ are different, varying periodically with time. When the time difference is half a period, any two velocity profiles have the same amplitudes but inverse directions.

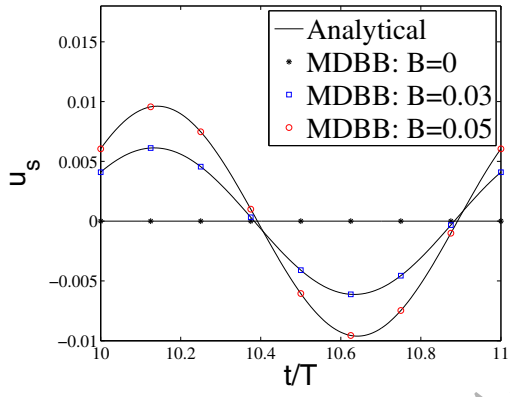


Figure 17: Slip velocity of the Womersley flow at different time.

As shown in Fig.16, the slip length has great effect on the velocity profiles. In Fig.17, the slip velocities of the Womersley flow are depicted as functions of time in tenth period. It can be observed that the slip velocities are zero at any time for $B$ =0, while the slip velocities for $B$ =0.03 and 0.05 vary with time. This phenomenon can be explained by the Navier's slip model Eq.(21). If the slip length is bigger than zero, the slip velocity varies with the velocity gradient at the normal direction of the wall. For the unsteady Womersley flow, the velocity gradient varies with time. So the slip velocities for $B$ =0.03 and 0.05 vary with time. The analytical solutions of the slip velocities at different time are also shown in Fig.17. Excellent agreements can be observed between the results predicted by the MDBB scheme and the analytical solutions.

The numerical results of the Womersley flow demonstrate the generality of our improved DBB schemes. Although the combination parameters are deduced based on the linear Couette flow, they are suitable for nonlinear flows with fine enough grid.

### *3.4. Cylindrical Couette flow with slip boundary*

The above simulations have tested the slip boundary conditions for liquid flow with simple straight walls. For complex flows with curved walls, there are no accurate relations between the combination parameters and the slip length. Without other better choices, we use the relations deduced based on the Couette flow to simulate the local flow near complex walls approximately [37, 38, 40, 41]. Among these slip boundary conditions, the specular

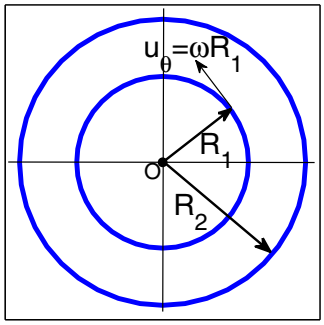


Figure 18: Schematic of cylindrical Couette flow.

reflection parts of the HBSR, MBSR, HDSR and MDSR are not computed locally, making it difficult to use these four schemes for curved boundaries [38]. On the contrary, the HDBB and MDBB schemes have the nature of local calculation. Results of the Poiseuille flow demonstrate that the MDBB scheme will introduce more discrete effects than the HDBB scheme. Therefore the HDBB scheme is employed to obtain boundary slip at curved walls in this subsection. The HDBB scheme specifies the unknown distribution function as [37]

$$f_i = s f_i^{eq} + (1-s)\bar{f}_{\bar{i}} \tag{45}$$

where $\bar{i}$ is the opposite direction of $i$.

The cylindrical Couette flow is a classical benchmark problem of complex flows and we take it to test the HDBB scheme for liquid slip at curved walls. As shown in Fig.18, two cylinders are concentric. The inner cylinder with radius $R_1$ rotates at a constant anticlockwise angular velocity $\omega$ and the non-equilibrium extrapolation method is adopted on it. The outer one with $R_2$ keeps stationary and the slip boundary condition is employed on it. The density at the wall is given following the former's work [37]. In a cylindrical polar coordinate ($R$, $\theta$), this flow can be expressed as

$$\frac{d^2 u_\theta}{dR^2} + \frac{d(u_\theta/R)}{dR} = 0 \tag{46}$$

where $u_\theta$ is the tangential velocity and $R$ is the radius.

With the linear slip boundary condition Eq.(21), the velocity at $R = R_2$

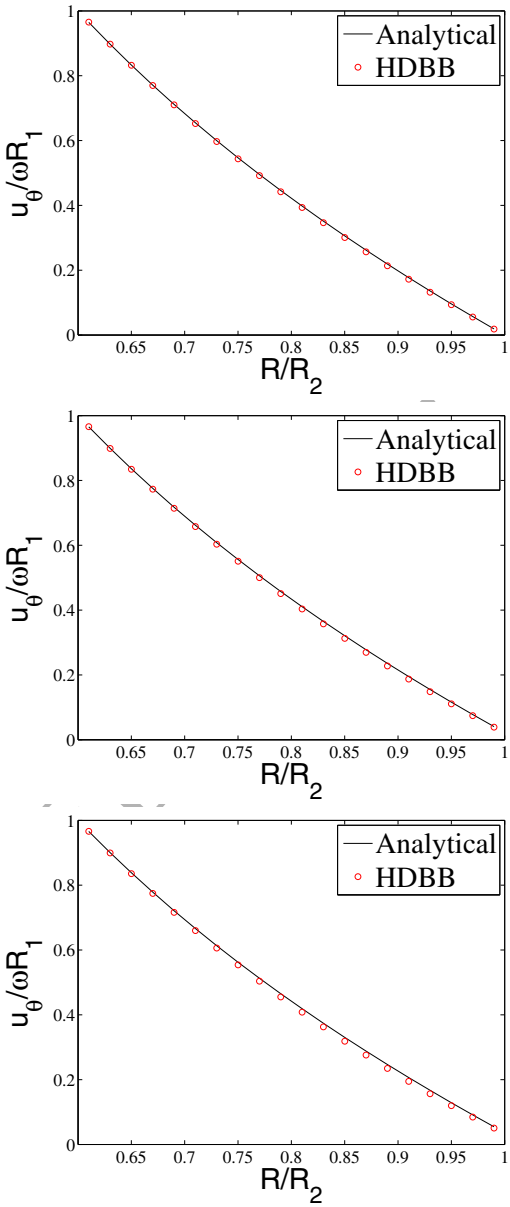


Figure 19: Tangential velocity of the cylindrical Couette flow ( $b/(R_2 - R_1)$ =0, 0.03 and 0.05 respectively from the top to the bottom, $R_2/R_1 = 5/3$).

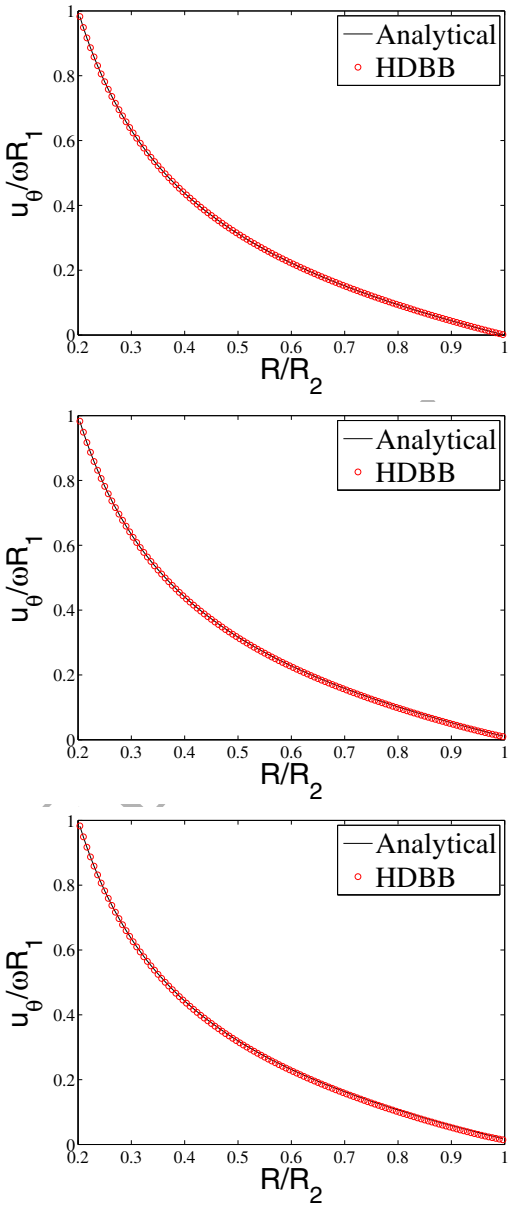


Figure 20: Tangential velocity profiles of the cylindrical Couette flow ( $b/(R_2 - R_1)$ =0, 0.03 and 0.05 from the top to the bottom, $R_2/R_1 = 5/1$).

can be given as

$$u_\theta|_{R=R_2} = -b(\frac{du_\theta}{dR} - \frac{u_\theta}{R})|_{R=R_2} \tag{47}$$

Then, the theoretical velocity profiles can be calculated as

$$\frac{u_\theta}{\omega R_1} = \frac{1}{(AR_1 - \frac{1}{R_1})}(AR - \frac{1}{R}) \tag{48}$$

with $A = \frac{1}{R_2^2}(1 - \frac{2b}{R_2})$.

In our work, we set $R_1$=30, $R_2$=50, $\omega = 10^{-3}$ and $\tau$=0.6. The combination parameters are calculated according to Eq.(25). If $b/(R_2 - R_1)$ is no more than 0.005, the combination parameters are within [0, 1]. Besides, if $b/(R_2 - R_1)$ is larger than 0.005, the combination parameters will fall into the range of [1, 2]. Three sets of simulations with $b/(R_2 - R_1)$ =0, 0.03, 0.05 are conducted to test our improved HDBB scheme for curved walls. Fig.19 depicts the numerical velocity profiles and the analytical results given by Eq.(48). It is noted that the numerical results agree well with the analytical solutions.

We notice that the cylinder Couette flow with $R_1$=30 and $R_2$=50 is close to a linear flow. In order to test our slip boundary condition for flows with higher non-linearity, we simulate the cylinder Couette flow with $R_1$=30 and $R_2$=150. The results are shown in Fig.20. It can be observed that the velocity profiles obtained by the HDBB scheme are consistent with the analytical results given by Eq.(48). Fig.19 and Fig.20 also show that the differences between the numerical results and the analytical solutions become a little bigger with increased slip length. After all, the local flow around the curved wall is approximated with the linear flow and some differences can not be avoided. Fig.19 and Fig.20 suggest that the differences are very small and the results can be acceptable. Therefor, we can conclude that the improved HDBB scheme with Eq.(25) is suitable for the simulation of liquid slip with curved walls.

## 4. Conclusion

The slip length defined firstly by the Naviers slip model is a characteristic quantity describing the slip property of a specific liquid-solid surface. In this work, we have introduced two half-way schemes and two modified schemes with adjustable slip length for the lattice Boltzmann simulation of liquid

flow. Through theoretical analysis of the simple unidirectional liquid flow, we discover that the half-way schemes are equivalent and the modified schemes are also equivalent. Based on the principle of equivalence, ranges of the combination parameters of the HDSR, HDBB, MDSR and MDBB schemes are improved from [0,1] to [0,2]. This improvement is beneficial to obtain a wider range of slip length. Moreover, relations between the combination parameters and the slip length are deduced strictly in theory. Among these slip boundary conditions, the HDBB and MDBB schemes are suitable for the simulation of liquid flows with complex geometries for the nature of their local computations.

The simulations of the Couette flow and the Poiseuille flow show that the theoretical analyses are reliable and accurate. For linear flow, the combination parameter is decided by the relaxation time and the given slip length without discrete effects. But for non-linear flow, discrete effects exist in all four slip boundary conditions. The discrete effects influence not only the range of the simulated slip length but also the accuracy of the numerical results. If the grid is fine enough, the discrete effects will be significantly reduced and even can be ignored. So the combination parameters deduced based on the linear Couette flow are suitable for nonlinear flow with enough fine grid.

The generality of our method is verified by the simulation of the Womersley flow, which is unsteady and strongly nonlinear. Simulations show that the velocity profiles of the Womersley flow vary with time. And the slip length has great effect on the velocity profiles. The slip velocities are zero at any time for $B$ =0, while the slip velocities for $B = 0.03$ and 0.05 vary with time. The numerical results are in excellent agreements with the analytical solutions.

In addition, the HDBB scheme is applied to simulate the curved walls of the cylindrical Couette flow for its local calculations and less discrete effects than the modified schemes. The local flow near the curved wall is approximated by the Couette flow. The numerical results demonstrate the accuracy and reliability of the improved HDBB scheme.

These boundary conditions with adjustable slip length are proposed and analysed for the two-dimensional simulation with the LBGK model. Following our procedure, present methods can be easily extended to the three-dimensional simulation and the multiple relaxation time (MRT) model. Besides, the potential of these methods in turbulence modeling needs to be explored. We will focus on these problems in the future work.

**Acknowledgements**

We acknowledge the financial support from the National Natural Science Foundation of China (Grant No.51475179 and No.51679099), and the Fundamental Research Funds for the Central Universities HUST. 2016JCTD207.

**References**

**References**

[1] X. Nie, G. D. Doolen, S. Chen, Lattice Boltzmann simulations of fluid flows in MEMS, Journal of Statistical Physics 107 (1) (2002) 279–289.

[2] C. Lim, C. Shu, X. Niu, Y. Chew, Application of lattice Boltzmann method to simulate microchannel flows, Physics of Fluids 14 (7) (2002) 2299–2308.

[3] T. Darmanin, F. Guittard, Recent advances in the potential applications of bioinspired superhydrophobic materials, Journal of Materials Chemistry A 2 (39) (2014) 16319–16359.

[4] M. A. Samaha, H. V. Tafreshi, M. GadelHak, Superhydrophobic surfaces: From the lotus leaf to the submarine, Comptes Rendus Mécanique 340 (1) (2012) 18–34.

[5] G. B. Hwang, A. Patir, K. Page, Y. Lu, E. Allan, I. P. Parkin, Buoyancy increase and drag-reduction through a simple superhydrophobic coating, Nanoscale 9 (22) (2017) 7588.

[6] S. Wang, L. Feng, L. Jiang, One-step solution-immersion process for the fabrication of stable bionic superhydrophobic surfaces, Advanced Materials 18 (6) (2006) 767–770.

[7] X. Hong, X. Gao, L. Jiang, Application of superhydrophobic surface with high adhesive force in no lost transport of superparamagnetic microdroplet, Journal of the American Chemical Society 129 (6) (2007) 1478–1479.

[8] W. Zhang, Y. Zhu, X. Liu, D. Wang, J. Li, L. Jiang, J. Jin, Salt-induced fabrication of superhydrophilic and underwater superoleophobic PAA-g-PVDF membranes for effective separation of oil-in-water emulsions, Angewandte Chemie 53 (3) (2014) 856–860.

[9] Y. Xue, Y. Wu, X. Pei, H. Duan, Q. Xue, F. Zhou, How solid-liquid adhesive property regulates liquid slippage on solid surfaces?, Langmuir 31 (1) (2015) 226–32.

[10] R. S. Voronov, D. V. Papavassiliou, L. L. Lee, Review of fluid slip over superhydrophobic surfaces and its dependence on the contact angle, Industrial & Engineering Chemistry Research 47 (8) (2008) 2455–2477.

[11] D. Schäffel, K. Koynov, D. Vollmer, H. J. Butt, C. Schönecker, Local flow field and slip length of superhydrophobic surfaces, Physical Review Letters 116 (13) (2016) 134501.

[12] M. A. Samaha, H. Vahedi Tafreshi, M. GadelHak, Modeling drag reduction and meniscus stability of superhydrophobic surfaces comprised of random roughness, Physics of Fluids 23 (1) (2011) 012001.

[13] C. Lee, C. H. Choi, C. J. Kim, Superhydrophobic drag reduction in laminar flows: a critical review, Experiments in Fluids 57 (12) (2016) 176.

[14] C. L. M. H. Navier, Mémoire sur les lois du mouvement des fluides, Mémoires de ÍAcadémie Royale des Sciences de ÍInstitut de France 6 (1) (1823) 389–416.

[15] J. P. Rothstein, Slip on superhydrophobic surfaces, Annual Review of Fluid Mechanics 42 (1) (2010) 89–109.

[16] A. Karimipour, A. D'Orazio, M. S. Shadloo, The effects of different nano particles of Al2O3 and Ag on the MHD nano fluid flow and heat transfer in a microchannel including slip velocity and temperature jump, Physica E: Low-dimensional Systems and Nanostructures 86 (1) (2017) 146–153.

[17] C. Neto, D. R. Evans, E. Bonaccurso, H. J. Butt, V. S. Craig, Boundary slip in Newtonian liquids: a review of experimental studies, Reports on Progress in Physics 68 (12) (2005) 2859.

[18] A. Karimipour, M. H. Esfe, M. R. Safaei, D. T. Semiromi, S. Jafari, S. N. Kazi, Mixed convection of copper-water nanofluid in a shallow inclined lid driven cavity using the lattice Boltzmann method, Physica A: Statistical Mechanics & Its Applications 402 (10) (2014) 150–168.

[19] M. Esfandiary, B. Mehmandoust, A. Karimipour, H. A. Pakravan, Natural convection of Al2O3-water nanofluid in an inclined enclosure with the effects of slip velocity mechanisms: Brownian motion and thermophoresis phenomenon, International Journal of Thermal Sciences 105 (1) (2016) 137–158.

[20] Z. Guo, B. Shi, T. Zhao, C. Zheng, Discrete effects on boundary conditions for the lattice Boltzmann equation in simulating microscale gas flows, Physical Review E 76 (5) (2007) 056704.

[21] C. K. Aidun, J. R. Clausen, Lattice Boltzmann method for complex flows, Annual Review of Fluid Mechanics 42 (1) (2010) 439–472.

[22] X. He, Q. Zou, L. Luo, M. Dembo, Analytic solutions of simple flows and analysis of nonslip boundary conditions for the lattice Boltzmann BGK model, Journal of Statistical Physics 87 (1) (1997) 115–136.

[23] S. Succi, Mesoscopic modeling of slip motion at fluid-solid interfaces with heterogeneous catalysis, Physical Review Letters 89 (6) (2002) 064502.

[24] A. Karimipour, A. H. Nezhad, A. D'Orazio, E. Shirani, Investigation of the gravity effects on the mixed convection heat transfer in a microchannel using lattice Boltzmann method, International Journal of Thermal Sciences 54 (19) (2012) 142–152.

[25] S. Ansumali, I. V. Karlin, Kinetic boundary conditions in the lattice Boltzmann method, Physical Review E 66 (2) (2002) 026311.

[26] G. Tang, W. Tao, Y. He, Lattice Boltzmann method for gaseous microflows using kinetic theory boundary conditions, Physics of Fluids 17 (5) (2005) 058101.

[27] Z. Guo, T. Zhao, Y. Shi, Physical symmetry, spatial accuracy, and relaxation time of the lattice Boltzmann equation for microgas flows, Journal of Applied Physics 99 (7) (2006) 074903.

[28] Z. Chai, Z. Guo, L. Zheng, B. Shi, Lattice Boltzmann simulation of surface roughness effect on gaseous flow in a microchannel, Journal of Applied Physics 104 (1) (2008) 014902.

[29] F. Verhaeghe, L. Luo, B. Blanpain, Lattice Boltzmann modeling of microchannel flow in slip flow regime, Journal of Computational Physics 228 (1) (2009) 147–157.

[30] M. Sbragaglia, S. Succi, Analytical calculation of slip flow in lattice Boltzmann models with kinetic boundary conditions, Physics of Fluids 17 (9) (2005) 093602.

[31] A. Karimipour, A. H. Nezhad, A. D'Orazio, M. H. Esfe, M. R. Safaei, E. Shirani, Simulation of copper–water nanofluid in a microchannel in slip flow regime using the lattice Boltzmann method, European Journal of Mechanics 49 (1) (2015) 89–99.

[32] A. Karimipour, New correlation for nusselt number of nanofluid with Ag/Al2O3/Cu nanoparticles in a microchannel considering slip velocity and temperature jump by using lattice Boltzmann method, International Journal of Thermal Sciences 91 (1) (2015) 146–156.

[33] K. Wang, Y. Zhang, Y. Yu, G. Hou, F. Zhou, Y. Wu, Simulation of boundary slip on a liquid-solid surface based on the lattice Boltzmann method, Scienceasia 41 (2) (2015) 130–135.

[34] N. K. Ahmed, M. Hecht, A boundary condition with adjustable slip length for lattice Boltzmann simulations, Journal of Statistical Mechanics: Theory & Experiment 2009 (5) (2009) 1255–1274.

[35] O. Švec, J. Skoček, Simple Navier's slip boundary condition for the non-Newtonian lattice Boltzmann fluid dynamics solver, Journal of Non-Newtonian Fluid Mechanics 199 (1) (2013) 61–69.

[36] K. Wang, Z. Chai, G. Hou, W. Chen, S. Xu, Slip boundary condition for lattice Boltzmann modeling of liquid flows, Computers & Fluids 161 (1) (2018) 60–73.

[37] Z. Guo, B. Shi, C. Zheng, Velocity inversion of micro cylindrical couette flow: A lattice Boltzmann study, Computers & Mathematics with Applications 61 (12) (2011) 3519–3527.

[38] S. Tao, Z. Guo, Boundary condition for lattice Boltzmann modeling of microscale gas flows with curved walls in the slip regime, Physical Review E 91 (4) (2015) 043305.

[39] Z. Guo, C. Zheng, B. Shi, Discrete lattice effects on the forcing term in the lattice Boltzmann method, Physical Review E 65 (4) (2002) 046308.

[40] C. Shu, X. Niu, Y. Chew, A lattice Boltzmann kinetic model for microflow and heat transfer, Journal of Statistical Physics 121 (1-2) (2005) 239–255.

[41] X. Niu, C. Shu, Y. Chew, Numerical simulation of isothermal micro flows by lattice Boltzmann method and theoretical analysis of the diffuse scattering boundary condition, International Journal of Modern Physics C 16 (12) (2005) 1927–1941.